PROTEIN STRUCTURE AND FOLDING:

The Structure of Human β-Defensin-1: NEW INSIGHTS INTO STRUCTURAL PROPERTIES OF β-DEFENSINS

David M. Hoover, Oleg Chertov and Jacek Lubkowski

J. Biol. Chem. 2001, 276:39021-39026.
doi: 10.1074/jbc.M103830200 originally published online August 2, 2001

THE JOURNAL OF BIOLOGICAL CHEMISTRY Vol. 276, No. 42, Issue of October 19, pp. 39021–39026, 2001
Printed in U.S.A.

The Structure of Human β-Defensin-1

NEW INSIGHTS INTO STRUCTURAL PROPERTIES OF β-DEFENSINS*

Received for publication, April 30, 2001, and in revised form, July 6, 2001
Published, JBC Papers in Press, August 2, 2001, DOI 10.1074/jbc.M103830200

David M. Hoover‡, Oleg Chertov§ and Jacek Lubkowski‡¶

From the ‡Macromolecular Crystallography Laboratory and the §Intramural Research Support Program, LMI, SAIC Frederick, NCI at Frederick, National Institutes of Health, Frederick, Maryland 21702

Defensins are a class of small cationic peptides found in higher organisms that serve as both antimicrobial and cell signaling molecules. The exact mechanism of the antimicrobial activity of defensins is not known, but two models have been postulated, one involving pore formation and the other involving nonspecific electrostatic interaction with the bacterial membrane. Here we report the high resolution structures of human β-defensin-1 (hBD1) in two crystallographic space groups. The structure of a single molecule is very similar to that of human β-defensin-2 (hBD2), confirming the presence of an N-terminal α-helix. However, while the packing of hBD1 is conserved across both space groups, there is no evidence for any larger quaternary structure similar to octameric hBD2. Furthermore, the topology of hBD1 dimers that are formed between monomers in the asymmetric unit is distinct from both hBD2 and other mammalian α-defensins. The structures of hBD1 and hBD2 provide a first step toward understanding the structural basis of antimicrobial and chemotactic properties of human β-defensins.

Defensins comprise a subclass of small, cysteine-rich, cationic antimicrobial peptides produced by higher organisms (1). Mammalian defensins are further classified into α-defensins and β-defensins based on both precursor and gene structure, as well as a pattern of six cysteines forming three disulfide bonds and an overall length of 25–45 amino acids. α-Defensins have broad antimicrobial activity against Gram-negative and Gram-positive bacteria, fungi, and enveloped viruses (2). β-Defensins are mainly active against Gram-negative bacteria and yeast (3), although many also have activity against Gram-positive bacteria. Both α- and β-defensins are not only antimicrobial, but serve also as immunostimulating agents (4). Recently, a cyclic peptide of 18 amino acids with three disulfides from macaque leukocytes was discovered and termed θ-defensin (5).

Three β-defensins, termed β-defensin-1 (hBD1), -2 (hBD2), and -3 (hBD3),[1] have been identified in humans. While these proteins possess sequence similarities, their properties are relatively distinct. hBD1 displays antimicrobial activity against Gram-positive and Gram-negative bacteria, as well as adenovirus (6), but its activity is easily inhibited by salt and diminishes in the presence of >40 mM NaCl. This salt-related inhibition is reduced with high concentrations of protein (7). hBD2 is functionally more targeted than hBD1, being active against Gram-negative bacteria and yeast (*Candida albicans*), but not against Gram-positive bacteria (3). hBD2 is also approximately ten times more potent than hBD1 against *Escherichia coli* (7). Furthermore, the gene structures of hBD1 and hBD2 are distinct, based on intron size, sites of expression, and elements of genetic regulation (8). hBD3 seems to be functionally distinct from both hBD1 and hBD2 in that its expression is inhibited by corticosteroids (9) and is active against both Gram-positive and Gram-negative bacteria with little to no effect of salt on its activity (10).

An alignment of known β-defensin sequences shows that almost all residues that are highly conserved play structural roles. Most other residues are highly variable. Because of this discrepency, the difference in properties between hBD1 and hBD2 cannot easily be ascribed to individual residues in their amino acid sequences. Native hBD1 is shorter by three residues at the N terminus and by one residue at the C terminus, as compared with hBD2. It should be noted that in the case of human neutrophil peptide-2 (hNP2), a member of the α-defensin family, addition of a single cationic residue at the N and C termini dramatically enhanced antimicrobial activity, while the addition of anionic residues rendered the molecule totally inactive (11). However, an N-terminal truncation of the first three residues of hBD2 did not affect its activity against *E. coli* (12).

Recently, the published high resolution crystal structure of hBD2 showed that hBD2 monomers can form an octameric assembly with uniform positive charge on its outer surface (13). However, an NMR structure recently reported for hBD2 showed that it does not oligomerize in solution at concentrations up to 2.4 mM (14). It was postulated, however, that oligomers of hBD2 similar to those found in crystals could occur on the surface of bacterial membranes. Although hBD1 is similar to hBD2 in sequence, its properties are distinctly different. In an attempt to explain the differences in properties between hBD1 and hBD2, we solved the crystal structure of hBD1 at high resolution and in two different crystal forms.

EXPERIMENTAL PROCEDURES

Crystallization—The protein was obtained from PeproTech (Rocky Hill, NJ). The homogeneity of the preparation was verified by matrix-assisted laser desorption/ionization time-of-flight mass spectroscopy. Monoclinic crystals were obtained by hanging-drop diffusion with equal

* This work was supported in part by the Intramural AIDS Targeted Antiviral Program of the Office of the Director, National Institutes of Health (to J. L.) and by Contract N01-CO-56000 from NCI, National Institutes of Health (to O. C.). The costs of publication of this article were defrayed in part by the payment of page charges. This article must therefore be hereby marked "*advertisement*" in accordance with 18 U.S.C. Section 1734 solely to indicate this fact.

The atomic coordinates and structure factors (code PDB 1IJU and PDB 1IJV) have been deposited in the Protein Data Bank, Research Collaboratory for Structural Bioinformatics, Rutgers University, New Brunswick, NJ (http://www.rcsb.org/).

¶ To whom correspondence should be addressed: Macromolecular Crystallography Laboratory, NCI at Frederick, NIH, P. O. Box B, Ft. Detrick, Frederick, MD 21701. Tel.: 301-846-5494; Fax: 301-846-7101; E-mail: jacek@ncifcrf.gov.

[1] The abbreviations used are: hBD, human β-defensin; a.u., asymmetric unit; hNP, human neutrophil peptide; NP, neutrophil peptide; r.m.s.d., root mean square deviation.

TABLE I
Data and refinement statistics

Data set	Orthorhombic		Monoclinic
Wavelength (Å)	0.920	0.917	0.979
Space group	$P2_12_12_1$		$P2_1$
Unit cell (Å)	a = 27.121 b = 47.243 c = 53.853	a = 27.083 b = 47.234 c = 53.849	a = 44.817 b = 26.814 c = 58.834 β = 102.13
Resolution range[a] (Å)	25.0–1.20 (1.24–1.20)	30.0–1.10 (1.14–1.10)	25.0–1.40 (1.45–1.40)
R_{merge}[b,c]	0.039 (0.250)	0.077 (0.460)	0.042 (0.242)
Total no. of observations	87,673	101,911	87,587
No. of independent observations	21,821	27,703	26,325
Completeness[b] (%)	97.3 (90.2)	95.8 (87.9)	95.5 (64.1)
Average $1/\sigma_1$[b,c]	32.1 (4.0)	16.0 (2.0)	27.2 (2.5)
Refinement			
No. of reflections			
Working set	38,900		20,061
Test set	760		1,019
Resolution range (Å)	20.0–1.20		20.0–1.40
R_{work}, R_{free}[d]			
All reflections	0.157, 0.193		0.175, 0.218
For $F > 4^*\sigma_F$	0.132, 0.163		0.160, 0.199
Total no. of non-hydrogen atoms	796		1505
Water molecules	176		270
Heterogen atoms	17		47
Average B-factor (Å^2)			
All non-hydrogen atoms	9.9		21.4
Protein atoms	9.4		20.7
No. of disordered residues	8		15
r.m.s.d. values from ideality			
Bonds (Å)	0.016		0.010
Angles distances (Å)	0.035		0.028
Plane distances (Å)	0.028		0.028

[a] The highest resolution shell ranges, as determined using DENZO (16), are shown in parentheses.
[b] Values shown in parentheses correspond to the high resolution shell.
[c] $R_{merge} = \Sigma|I_n - \langle I\rangle|/\Sigma\langle I\rangle$.
[d] $R_{work} = \Sigma||F_o(h)| - k|F_o(h)||/\Sigma|F_o(h)|$; $R_{free} = \Sigma(h)\epsilon T|\{|F_o(h)| - k|F_o(h)|\}|/\Sigma_{(h)\epsilon T}|F_o(h)|$, where T represents a test set of reflections (~5–8% of total, chosen at random) not used in the refinement.

volumes of concentrated protein (20 mg/ml after dissolving lyophilized protein in water) and reservoir solution containing 30% polyethylene glycol 4000, 15% glycerol, 0.1 M $(NH_4)_2SO_4$, 0.1 M NaOAc, pH 4.6. Orthorhombic crystals were grown under the same conditions, except that the reservoir solution contained an additional 0.5 M KBr. The orthorhombic form belongs to space group $P2_12_12_1$ with cell constants a = 27.12 Å, b = 47.24 Å, and c = 53.85 Å. The monoclinic form belongs to space group $P2_1$ with cell constants a = 44.82 Å, b = 26.81 Å, c = 58.83 Å, and β = 102.13°. Both crystal forms have very similar morphologies of diamond-shaped plates. The presence of KBr in the crystallization mixture always induced the appearance of orthorhombic crystals. Only the monoclinic crystals mentioned above (or triclinic crystals)[2] have been obtained in the absence of bromide. Addition of KBr to the crystallization mixture was not intended to generate novel crystal forms of hBD1, but rather to derivatize monoclinic crystals with Br^- anions. Such a procedure was described previously to collect x-ray data with bromine anomalous signal suitable for structure solution (13, 15). Despite their very small dimensions (0.08 × 0.08 × 0.03 mm^3), crystals of both forms proved to diffract very well.

Data Collection and Processing—Data were collected using crystals taken directly from the hanging droplet and frozen in the 100 K nitrogen stream. Addition of cryoprotectant was not necessary due to the presence of 15% glycerol in the crystallization mixture. X-ray data for both crystal forms were collected at beamline X9B, National Synchrotron Light Source, Brookhaven National Laboratory using an ADSC Quantum 4 CCD detector. The images were indexed, processed, merged, and scaled using DENZO and SCALEPACK (16). The data collection statistics are shown in Table I. The data set collected for orthorhombic crystals using the wavelength 0.917 Å (extending to 1.10 Å resolution) was used to locate the positions of bromide sites. The anomalous differences for this data set, calculated by PHASES (17), were 5.8% (based on F^2) and 4.9% (based on F), at 1.1-Å resolution. Only very weak anomalous signal could be detected for the other data set collected for orthorhombic crystals at the wavelength of 0.920 Å (extending to 1.20 Å resolution), and thus it was not included in the structure solution and phase refinement. However, the lack of the anomalous signal resulted in slightly better statistics during the data reduction (see Table I), and consequently these data were used during structural refinement.

Structure Solution and Refinement of the Orthorhombic Form—The positions of anomalous scatters (Br^-) were identified using the program SHELXS (18). Reflections within the resolution range of 20–1.5 Å were used from the data set collected at the wavelength of 0.917 Å. Three major and three minor sites were identified, and their positions were further refined using program SHARP (19). During this refinement, phases were subsequently extended to full experimental resolution range (20–1.1 Å). Subsequent phase modification was performed with program DM (20). Because the handedness of the calculated phases was unknown, both the original positions of the sites (x, y, z) and their negative inversions ($-x$, $-y$, $-z$) were refined. Although the resulting figures of merit for both coordinate sets were indistinguishable, the rate of convergence to a final solution for the correct set of coordinates using DM was significantly faster compared with its enantiomorph.

The final map from phase refinement and solvent flattening was easily interpretable (Fig. 1). An initial model was built manually using the program O (21), after identifying the electron density peaks corresponding to sulfur atoms that form disulfide bonds, and interpreting the sequence of the adjacent residues from the shape of electron density peaks. The asymmetric unit (a.u.) contained two protein chains of hBD1, and it was possible to place nearly all atoms (with a few exceptions of disordered side chains) in both monomers present in the a.u. Also, the electron density peaks corresponding to two SO_4^{2-} anions were very distinguishable. The initial model of hBD1 was refined with program CNS (22) at the resolution ranges 20.0–1.6 Å. Anomalous data were used for refinement, as the presence of anomalous scatterers (Br^-) in the model increased the value of R_{free} by 2–3% when the model was refined against merged data. During this refinement subsequent minor corrections were introduced manually to the model. Refinement of the structure at a resolution extending beyond 1.6 Å was conducted using program SHELXL (18). At this stage the presence of discrete disorder for eight residues was identified, and it was included in subsequent refinement. In the final steps, anisotropic displacement parameters for all atoms were individually refined. The final model, refined at the

[2] D. M. Hoover and J. Lubkowski, unpublished results.

1.2-Å resolution, consists of all protein residues (1 through 36 in each monomer) and 176 water molecules, two sulfate anions, six Br^- anions, and one K^+ cation. The *R* value for all reflections (20–1.2 Å) is 15.7% (R_{free} 19.3%).

Structure Solution and Refinement of the Monoclinic Form—The initial set of x-ray data for monoclinic crystals was collected using a conventional radiation source (wavelength 1.54178 Å) at 2.0 Å resolution. Analysis of this data by Patterson self-rotation searches showed the presence of a noncrystallographic 2-fold rotation axis perpendicular to the crystallographic 2-fold axis. A comparison of the unit cell parameters for both crystal forms and noncrystallographic symmetry indicated the presence of four independent monomers of hBD1 in the a.u. of monoclinic crystals. Our attempts to solve this structure by the method of molecular replacement, using models based on the structure of hBD2 (13), were unsuccessful. The molecular replacement approach was applied successfully, however, using the refined dimeric structure of hBD1 from the orthorhombic crystals as a search model. Solution of the monoclinic structure was obtained using program AMoRe (23). The model consisted of all non-hydrogen protein atoms with uniform B-factor values of 25 $Å^2$. Solvent atoms, as well as heterogen molecules, were removed from the model. During the molecular replacement searches a subset of the x-ray data collected for monoclinic crystals was used (Table I) corresponding to all reflections within the resolution range 9.0–2.6 Å. The solution for two dimers used as a model could be easily identified (correlation factor 45.7%, *R*-factor 46.0%). This solution was consistent with the noncrystallographic symmetry determined earlier.

Initial structural refinement was conducted with the program CNS (22), and the resolution was gradually extended to the range 20.0–1.8 Å. At this stage some fragments of the model were corrected manually, and many solvent sites were located. The locations of several SO_4^{2-} anions were also identified. Further refinement, at a resolution higher than 1.8 Å, was conducted with the program SHELXL (18). The final model was refined against data in the resolution range 20.0–1.4 Å. Anisotropic displacement parameters were applied only to the 31 sulfur atoms (24 cysteines and 7 SO_4^{2-}), as the resolution of the x-ray data was not as high as for the orthorhombic crystal form, and applying anisotropic displacement parameters to all atoms did not cause the R_{free} to improve. The final monoclinic model consists of all protein residues in all four crystallographically independent monomers and 270 water molecules, seven sulfate anions, and two molecules of glycerol. The *R* value for all reflections (20–1.4 Å) is 17.5% (R_{free} 23.1%).

RESULTS

Crystal Structure Solution—The crystal structure of the orthorhombic form was solved using the anomalous signal originating from the bromide anions at a single wavelength. The derivatization method used by us was the same as the one previously applied to hBD2 (13). This proves that under appropriate conditions (acidic pH),[3] Br^- ions bind readily and specifically to the protein, producing a halide derivative capable of strong anomalous dispersion of x-ray radiation. In contrast to the previously described structure of hBD2, in the present study only one Br^- derivative data set at a single wavelength was utilized during the phasing procedure. Despite the relatively limited experimental information, the high quality and resolution of the x-ray data resulted in very good electron density maps (Fig. 1). Although we did not use automatic model building that was previously employed for hBD2 (13), it was possible to build the initial protein structure quickly and easily. This example proves once more that the bromide derivatization method (15) using synchrotron radiation provides a powerful tool in rapid determination of high quality crystal structures and is an attractive component for structural genomics protocols (24).

Structural Features—The monomer of hBD1 displays a similar fold to that of hBD2 (13) and bovine β-defensin-12 (25). Residues His^2–Ser^7 form a short α-helix that flanks a three-stranded antiparallel β-sheet, with residues Gln^{11}–Leu^{13} forming strand β1, Ile^{23}–Cys^{27} forming strand β2, and Ala^{32}–Cys^{35} forming strand β3 (Fig. 2*A*). Residues Pro^{18}–Thr^{21} form a type II turn between strand β1 and β2, while residues Tyr^{28}–Lys^{31} form a type I′ turn between strand β2 and β3. Both residues Gln^{24} and Gly^{25} form hydrogen bonds with Cys^{34}, creating a β-bulge in strand β2. This β-bulge is conserved in all known β-defensin structures, and although its functional role is unknown, its presence is highly correlated with the sequence G-*X*-C (residues 32–34 in hBD1), a motif that is conserved in both α- and β-defensins. The protein is stabilized by three disulfides (Cys^5–Cys^{34}, Cys^{12}–Cys^{27}, Cys^{17}–Cys^{35}). Analysis of structural motifs was done using the program PROMOTIF (26).

The overall fold is very well defined and conserved among all monomers in both crystal forms of hBD1 (Fig. 2*B*). The average B-factors are very low ranging from 9.6 $Å^2$ for the backbone atoms in the chain A of orthorhombic form to 25.0 $Å^2$ for the side chains atoms of the chain D in the monoclinic form. Ramachandran plots (27), calculated using the program PROCHECK (28), show the conformations of all residues to be located within allowed regions. Although conformations of all residues are clearly defined by the experimental electron density, multiple conformations can be assigned for several residues. These include Ser_A^7, Ser_A^8, Asn_B^4, and Ser_B^7 in the orthorhombic structure and Ser_A^7, Ser_A^8, Ser_B^8, Ser_B^{15}, Ile_B^{23}, Ser_C^7, Ile_C^{19}, Ser_D^7, Ser_D^8, as well as fragment Tyr_D^{14}-Pro_D^{18}

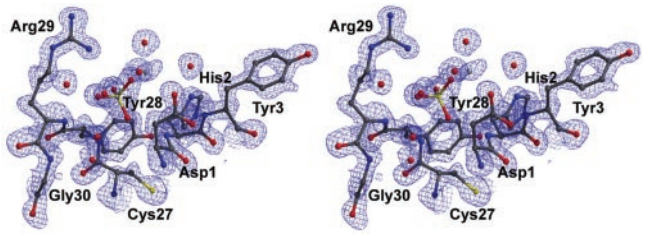

FIG. 1. **Experimental electron density map, contoured at 0.97 σ.** This fragment of the hBD1 model is taken from the fully refined structure. Very good agreement is found between the experimental electron density peaks and the atoms, including water molecules and a sulfate anion. This figure was generated using programs BOBSCRIPT (34) and POV-Ray (www.povray.org).

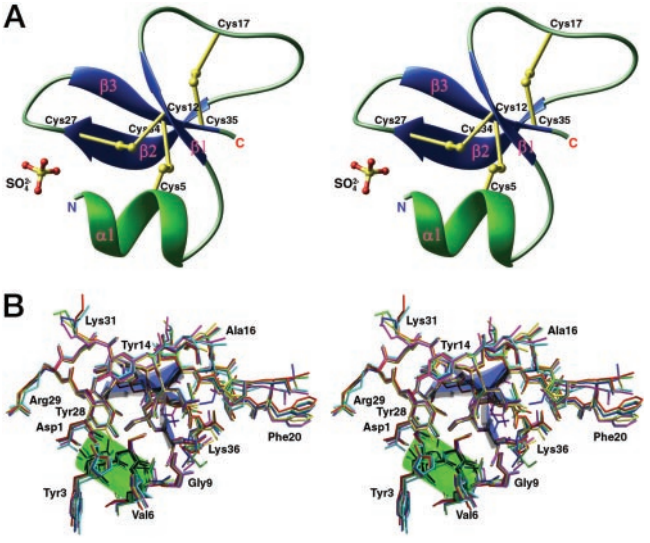

FIG. 2. **Stereo drawing of the hBD1 monomer.** *A*, the three-stranded anti-parallel β-sheet is shown in *blue*, while the flanking α-helix is shown in *green*. Both termini and three disulfide bridges are also shown and labeled. The SO_4^{2-} ion located in vicinity of the N terminus is present in all monomers of both crystal forms. This figure was made using the program RIBBONS (35). *B*, superposition of six crystallographically independent monomers of hBD1 indicates extensive structural conservation of all residues. Locations of secondary structure elements are shown in form of a semitransparent *green cylinder* (α-helix) and *blue arrows* (β-strands).

[3] D. M. Hoover and J. Lubkowski, personal observations.

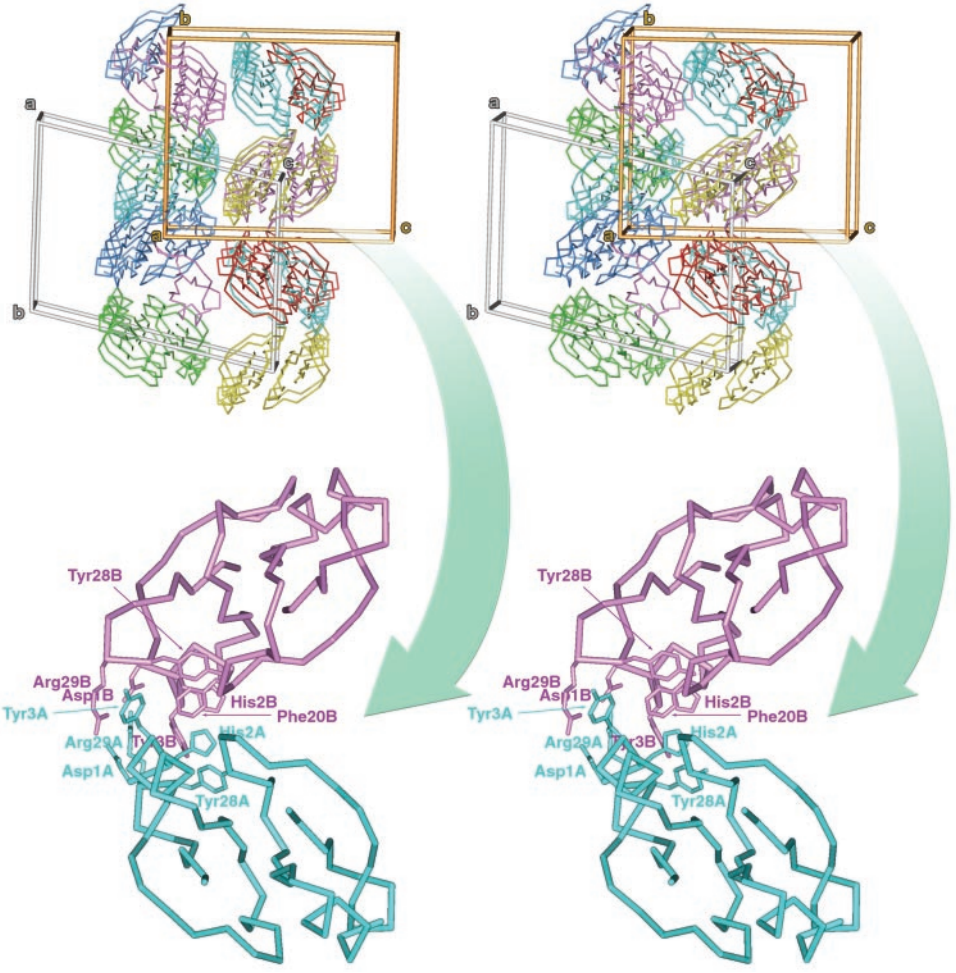

FIG. 3. **Crystal packing of hBD1 in two crystal forms.** Crystal assembly of hBD1 identified in the monoclinic form (unit cell shown in *gray*, Cα-traces of protein chains drawn in *green* for chain A, *blue* for chain B, *yellow* for chain C, and *red* for chain D) is aligned with that found in the orthorhombic form (unit cell shown in *brown*, while Cα-traces of protein chains A and B are shown in *cyan* and *magenta*, respectively). As seen, in both space groups molecules form nearly identical layers of dimers aligned along the *b*-axis (orthorhombic form) or *a*-axis (monoclinic form). One of such dimers, present in the orthorhombic unit cell, is showed enlarged in the lower part of this figure. Side chains of the residues stabilizing formation of this dimer are also depicted. Extensive similarity of the crystal packing in both crystal forms results from relationships between the unit cell parameters, which can be represented as: $a^{\text{orthorhombic}} \approx b^{\text{monoclinic}}$, $b^{\text{orthorhombic}} \approx a^{\text{monoclinic}}$, and $c^{\text{orthorhombic}} \approx \sin(\measuredangle a,b) \cdot c^{\text{monoclinic}}$. In the monoclinic space group, the adjacent layers are formed by exclusive pairs of monomers, AB and CD. While in the orthorhombic crystals the layers are related by the c/2-translation along the *c*-axis, the nonorthogonal geometry of the monoclinic symmetry results in a relative shift of consecutive layers along the *a*-axis, preventing simultaneous alignment of the contents of entire unit cells in both space groups.

in the monoclinic structure. In all monomers, the side chains of residues Lys^{22}, Gln^{24}, Lys^{31}, and Lys^{36} are quite mobile, as indicated by elevated B-factors.

The intermolecular contacts are relatively limited in both crystal forms. The highest value of the molecular surface buried upon the intermonomer interaction was found to be 343 $Å^2$/monomer for the monoclinic form and 301 $Å^2$/monomer for the orthorhombic (compared with >500 $Å^2$ for hBD2). Furthermore, the largest interface is formed by symmetry mates of the same monomer (chain B in the monoclinic form), rather than by crystallographically independent molecules. With such small interfaces between the monomers, no particular quaternary structure of hDB1 can be unambiguously characterized.

Comparison of Both Crystal Forms—Although two crystal forms of hBD1, monoclinic and orthorhombic, have been analyzed, the crystal packing was found to be very similar among them. Despite the absence of clear quaternary structure in the crystals of hBD1, we could identify a common dimeric arrangement between the independent monomers in the a.u. Within the dimers, interactions are primarily through the side chains of aromatic residues, bringing His^2, Tyr^3, and Tyr^{28} of one monomer in direct vicinity of His^2, Tyr^3, Phe^{20}, and Tyr^{28} of the second monomer (Fig. 3). Additional stabilization is provided by two salt bridges between the side chains of Asp^1 from one monomer and Arg^{29} from the other. Formation of this slightly curved dimer (see *bottom* of Fig. 3) results in the burial of more than 300 $Å^2$ of molecular surface per each monomer. Adjacent dimers, being translated and rotated against each other, interact through their concave sides. In such an arrangement an infinite series of dimers form layers extending parallel to the *xy*-plane and conserved to both crystal forms, as shown in Fig. 3. While the concave surfaces of the dimers, formed primarily by hydrophobic and neutral residues, are buried in the layers, their convex sides are composed of positively charged residues. The resulting hBD1 layers, observed in both crystal forms, present a positive two-dimensional electrostatic surface.

In both crystal forms a sulfate is bonded to backbone nitrogens from His^2, Tyr^{28}, and Arg^{29}, as well as to the guanidinium group of Arg^{29} (Figs. 1 and 2). Within the dimer, two sulfate ions are located near each other; however, there is no direct

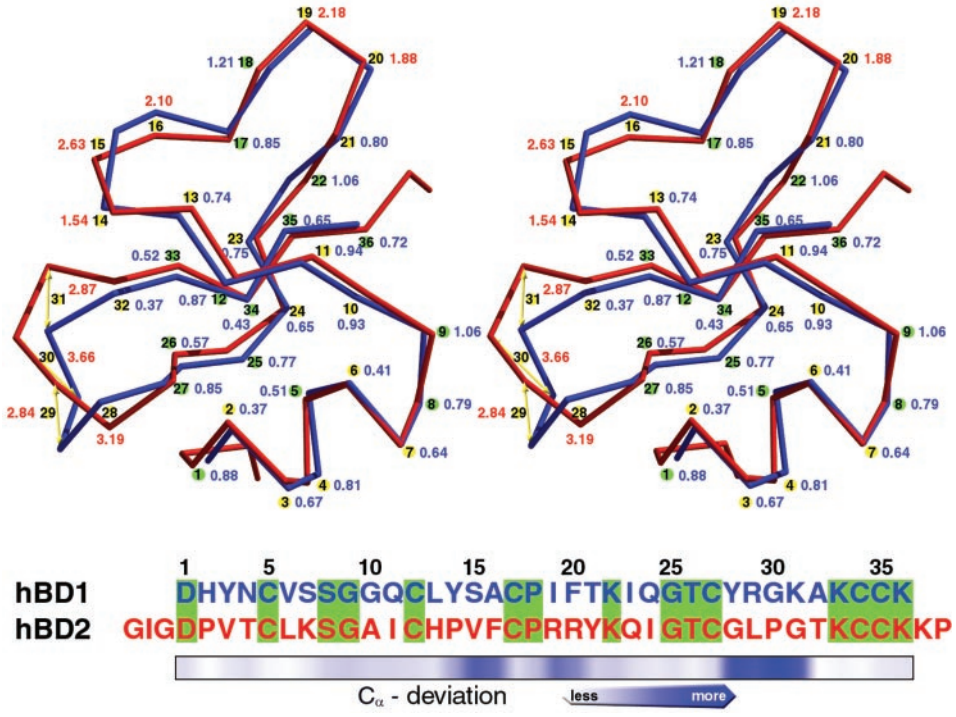

FIG. 4. **Alignment of hBD1 and hBD2.** The stereoscopic representation of Cα traces of both human β-defensins (hBD1 in *blue*, hBD2 in *red*) is shown in the *top* of the figure. The hBD1 residue numbers (shown in *black*) are assisted by the deviations (in Å) of corresponding Cα positions in two defensins (shown in *blue* and *red*). Deviations are the average values obtained from 120 alignments of 6 independent monomers of hBD1 and 20 independent monomers of hBD2. The highest values of deviations are shown in *red*. Residue numbers shown with *yellow circles* in the background indicate positions for which the discrepancies are larger than the r.m.s.d. calculated for the entire Cα traces, averaged over 120 independent alignments. The amino acid sequence alignment of hBD1 and hBD2 is shown at the *bottom*. Residues conserved for both proteins are printed on *green background*. The *shaded bar*, shown under the sequences, indicates structural conservation of Cα positions for corresponding residues and was generated using the deviations shown near the Cα traces.

contact between these anions. They interact through the network of hydrogen bonds, mediated by the water molecules. Additionally, a sulfate anion associated with one monomer is also hydrogen-bonded to Asp^{1} and Arg^{29} of the opposite monomer. The sulfates are held tightly within their sites, as evidenced by the ligation to backbone atoms with near ideal hydrogen bond lengths and the low concentrations of sulfate needed to crystallize the protein (~10–20 mM). The conservation of their position in two crystal forms may indicate a preformed binding site capable of binding phosphate groups, an essential part of bacterial membrane lipids.

Comparison with Human β-Defensin-2—The overall structure of the hBD1 monomer is very similar to that of hBD2 (Fig. 4). Both monomers can be superimposed with an overall root mean square deviation (r.m.s.d.) of ~0.6–0.7 Å using either Cα or all equivalent atoms. The secondary structure elements of both proteins are well conserved, with average deviations for individual Cα atoms being smaller than 0.5 Å. The major differences observed are within loops between strands β1 and β2 (residues Tyr^{14}–Phe^{20} in hBD1) and between strands β2 and β3 (residues Tyr^{28}–Lys^{31} in hBD1). Additionally, the amino acid sequence of hBD1 is shorter than that of hBD2, by three residues at the N terminus and two at the C terminus (see Fig. 4). In both proteins, conformations of the loop regions are conserved within all independent molecules, and they are not constrained by intermolecular contacts. Therefore, it is likely that in both cases the crystal structures represent native conformations.

There are three regions that differ significantly in structure between the monomers of hBD1 and hBD2, and these regions can be directly correlated with the differences of their amino acid sequences. The first region, a segment of four residues Leu^{13}-Tyr^{14}-Ser^{15}-Ala^{16} in hBD1 is substituted by His^{16}-Pro^{17}-Val^{18}-Phe^{19} in hBD2. The presence of His and Pro residues in hBD2 modifies both the electrostatic properties as well as geometric restraints of this solvent-exposed fragment. An even more dramatic difference is found by comparing Ile^{19}-Phe^{20}-Thr^{21} of hBD1 to the structurally equivalent Arg^{22}-Arg^{23}-Tyr^{24} in hBD2. This loop, located close to the C terminus, is highly positively charged in hBD2 but hydrophobic in hBD1. For the third structurally divergent region, we find differences to be rather opposite. The sequence consisting of two positively charged residues in hBD1, Tyr^{28}-Arg^{29}-Gly^{30}-Lys^{31}-Ala^{32}, is substituted by an electrically neutral and flexible (two Gly residues) fragment, Gly^{31}-Leu^{32}-Pro^{33}-Gly^{34}-Thr^{35} in hBD2.

Monomers of hBD1 were structurally superimposed onto the hBD2-type dimer seen in the crystal structures of hBD2 (13). Side chains of hBD1 residues in the modeled hBD2-type dimer showed close contacts and steric overlaps at the dimeric interface. Particularly unfavorable interactions are found for Tyr^{14} and the region Tyr^{28}–Lys^{31} as compared with equivalent residues in hBD2. These differences between hBD1 and hBD2 are possibly associated with their oligomerization properties.

DISCUSSION

Comparison of amino acid sequences and structures of different defensins and other related antimicrobial peptides reveals extensive similarities in these proteins. All contain a central β-sheet, composed of three antiparallel strands in α- and β-defensins, although only two strands are present in insect defensins (sapecins) (29). Human β-defensins share the presence of N-terminal α-helix with sapecins, while not with mammalian α-defensins. Although the three families of defensins contain their own distinct patterns of disulfide bonds,

the structural alignments show that positions of the disulfides occur within the same spatial regions of the protein. Last, in all three families of defensins, the fourth cysteine is preceeded by the sequence G-*X*-C. The backbone amide nitrogen and carbonyl oxygen of this cysteine forms hydrogen bonds to two residues in the second β-strand, causing the formation of structurally conserved β-bulge. It has been postulated that all defensins evolved from a single precursor, which was a β-defensin-like molecule (30). This postulate arose from the observation that the amino acid sequences and structures of β-defensins are more closely related to insect defensins than to mammalian α-defensins.

The most striking difference seen in comparisons of β-defensins (hBD1 and hBD2) with α-defensins (hNP3 (31) and rabbit NP1 and NP2 (32)) is the presence of an N-terminal helix in the former proteins. Although this helical region is also present in approximately the same position relative to the β-sheet in the antimicrobial peptides purothionine (wheat) and insect defensin A (33), in the NMR structure of bovine β-defensin (bovine β-defensin-12) the N-terminal residues are somewhat disordered, and the α-helix is not seen (25). Recently, the NMR structure of hBD2 confirms the presence of this α-helix in solution (14). The conservation of this structural element suggests that it may play a role in the antimicrobial activity of β-defensins; however, more definite conclusions require further mutational and structure studies.

There are currently two models describing the antimicrobial activity of defensins. One of them postulates the formation of multimeric pores within the bacterial membranes, and the other describes the activity of defensins in terms of nonspecific interactions between negatively charged moieties of the membrane and positive charges carried by side chains of defensin molecules. As shown previously, the crystal structure of hBD2 shows the monomers to form a compact octameric assembly (13). The uniform positive charge on the surface of the oligomer does not support pore formation within a membrane bilayer, and consequently the pore-forming model. Additionally, as discussed (13), hNP3-type dimers cannot be modeled using monomers of hBD2 due to steric collisions. Here, it is shown that hBD1 monomers cannot be arranged into either the crystallographic hBD2-type or hNP3-type dimers. The results described here, together with reports elucidating functional properties of defensins, appear insufficient to determine unambiguously the structural basis of either antimicrobial or chemotactic activity of β-defensins. Although there is little support for the mechanism proceeding via formation of membrane-embedded pores, understanding the membrane permeabilizing mechanism will require additional experiments aimed at correlating activities displayed by defensins with their structures.

Acknowledgments—We thank Dr. Alexander Wlodawer for his support, Dr. Zbigniew Dauter for his help with data collection, and Dr. Joost Oppenheim for advice and editorial suggestions.

REFERENCES

1. Epand, R. M., and Vogel, H. J. (1999) *Biochim. Biophys. Acta* **1462,** 11–28
2. Lehrer, R. I., and Ganz, T. (1996) *Ann. N. Y. Acad. Sci.* **797,** 228–239
3. Harder, J., Bartels, J., Christophers, E., and Schröder, J. M. (1997) *Nature* **387,** 861
4. Chertov, O., Yang, D., Howard, O. M., and Oppenheim, J. J. (2000) *Immunol. Rev.* **177,** 68–78
5. Tang, Y. Q., Yuan, J., Miller, C. J., and Selsted, M. E. (1999) *Infect. Immun.* **67,** 6139–6144
6. Gropp, R., Frye, M., Wagner, T. O., and Bargon, J. (1999) *Hum. Gene Ther.* **10,** 957–964
7. Singh, P. K., Jia, H. P., Wiles, K., Hesselberth, J., Liu, L., Conway, B. A., Greenberg, E. P., Valore, E. V., Welsh, M. J., Ganz, T., Tack, B. F., and McCray, P. B., Jr. (1998) *Proc. Natl. Acad. Sci. U. S. A.* **95,** 14961–14966
8. Diamond, G., and Bevins, C. L. (1998) *Clin. Immunol. Immunopathol.* **88,** 221–225
9. Duits, L. A., Rademaker, M., Ravensbergen, B., Van Sterkenburg, M. A., van Strijen, E., Hiemstra, P. S., and Nibbering, P. H. (2001) *Biochem. Biophys. Res. Commun.* **280,** 522–525
10. Harder, J., Bartels, J., Christophers, E., and Schröder, J. M. (2001) *J. Biol. Chem.* **276,** 5707–5713
11. Raj, P. A., Antonyraj, K. J., and Karunakaran, T. (2000) *Biochem. J.* **347,** 633–641
12. Bals, R., Wang, X., Wu, Z., Freeman, T., Bafna, V., Zasloff, M., and Wilson, J. M. (1998) *J. Clin. Invest.* **102,** 874–880
13. Hoover, D. M., Rajashankar, K. R., Blumenthal, R., Puri, A., Oppenheim, J. J., Chertov, O., and Lubkowski, J. (2000) *J. Biol. Chem.* **275,** 32911–32918
14. Sawai, M. V., Jia, H. P., Liu, L., Aseyev, V., Wiencek, J. M., McCray, P. B., Jr., Ganz, T., Kearney, W. R., and Tack, B. F. (2001) *Biochemistry* **40,** 3810–3816
15. Dauter, Z., Dauter, M., and Rajashankar, K. R. (2000) *Acta Crystallogr. Sect. D Biol. Crystallogr.* **56,** 232–237
16. Otwinowski, Z., and Minor, W. (1997) *Methods Enzymol.* **276,** 307–326
17. Furey, W., and Swaminathan, S. (1997) *Methods Enzymol.* **277,** 590–620
18. Sheldrick, G. M., and Schneider, T. R. (1997) *Methods Enzymol.* **277,** 319–344
19. de La Fortelle, E., and Bricogne, G. (1997) *Methods Enzymol.* **276,** 472–494
20. Cowtan, K. (1994) *Joint CCP4 ESF-EACBM Newsl. Protein Crystallogr.* **31,** 34–38
21. Jones, T. A., Zou, J. Y., Cowan, S. W., and Kjeldgaard, M. (1991) *Acta Crystallogr. Sect. A* **47,** 110–119
22. Brünger, A. T., Adams, P. D., Clore, G. M., DeLano, W. L., Gros, P., Grosse-Kunstleve, R. W., Jiang, J. S., Kuszewski, J., Nilges, M., Pannu, N. S., Read, R. J., Rice, L. M., Simonson, T., and Warren, G. L. (1998) *Acta Crystallogr. Sect. D Biol. Crystallogr.* **54,** 905–921
23. Navaza, J. (1994) *Acta Crystallogr. Sect. A* **50,** 157–163
24. Dauter, Z., Li, M., and Wlodawer, A. (2001) *Acta Crystallogr. Sect. D Biol. Crystallogr.* **57,** 239–249
25. Zimmermann, G. R., Legault, P., Selsted, M. E., and Pardi, A. (1995) *Biochemistry* **34,** 13663–13671
26. Hutchinson, E. G., and Thornton, J. M. (1996) *Protein Sci.* **5,** 212–220
27. Ramachandran, G. N., and Sasisekharan, V. (1968) *Adv. Protein Chem.* **23,** 283–438
28. Laskowski, R. A., MacArthur, M. W., Moss, D. S., and Thornton, J. M. (1993) *J. Appl. Crystallogr.* **26,** 283–291
29. Hanzawa, H., Shimada, I., Kuzuhara, T., Komano, H., Kohda, D., Inagaki, F., Natori, S., and Arata, Y. (1990) *FEBS Lett.* **269,** 413–420
30. Hughes, A. L. (1999) *Cell Mol. Life Sci.* **56,** 94–103
31. Hill, C. P., Yee, J., Selsted, M. E., and Eisenberg, D. (1991) *Science* **251,** 1481–1485
32. Pardi, A., Zhang, X. L., Selsted, M. E., Skalicky, J. J., and Yip, P. F. (1992) *Biochemistry* **31,** 11357–11364
33. Hwang, P. M., and Vogel, H. J. (1998) *Biochem. Cell Biol.* **76,** 235–246
34. Esnouf, R. M. (1997) *J. Mol. Graph. Model.* **15,** 132–133
35. Carson, M. (1991) *J. Appl. Crystallogr.* **24,** 958–961